Generation of abasic sites in DNA by singlet oxygen produced from a photocatalytic reaction

AUTHORS

Yuuhei Yamano[1], Kazumitsu Onizuka[1, 2, 3*], Okan Altan[1], Madoka Sasaki[1, 2], Ahmed Mostafa Abdelhady[1, 4], and Fumi Nagatsugi[1, 2*]

[1]Institute of Multidisciplinary Research for Advanced Materials, Tohoku University, 2-1-1 Katahira, Aoba-ku, Sendai, Miyagi 980-8577, Japan

[2]Department of Chemistry, Graduate School of Science, Tohoku University, Aoba-ku, Sendai 980-8578, Japan

[3]Division for the Establishment of Frontier Sciences of Organization for Advanced Studies, Tohoku University, Aoba-ku, Sendai, Miyagi 980-8577, Japan

[4]Department of Chemistry, Faculty of Science, Al-Azhar University, Nasr City, Cairo, Egypt

*To whom correspondence should be addressed. Tel: +81-22-217-5634; Fax: +81-22-217-5633;

Email: onizuka@tohoku.ac.jp, nagatugi@tohoku.ac.jp

GRAPHICAL ABSTRACT

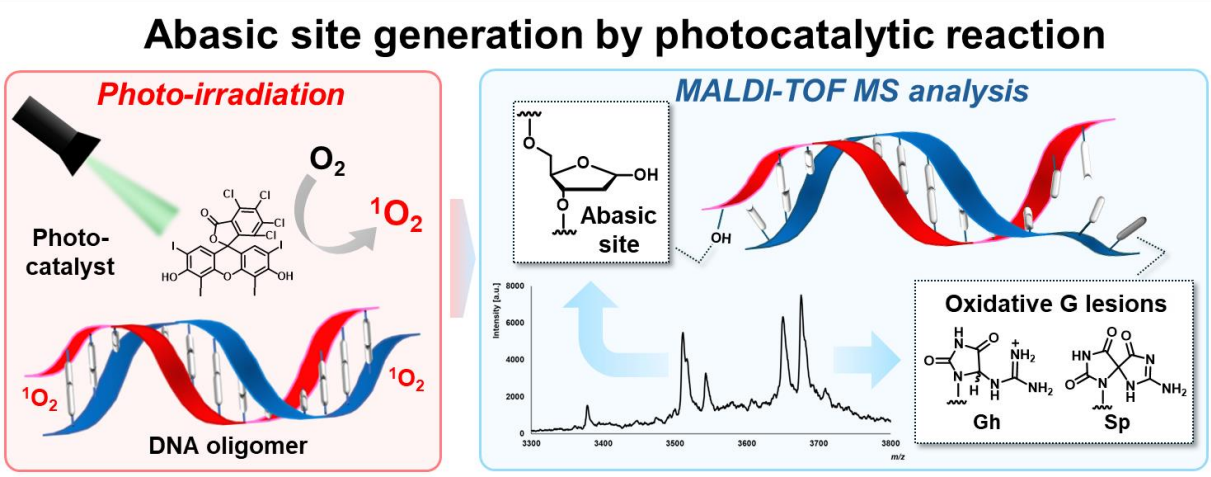

ABSTRACT

Stress factors such as photoreaction and inflammation are known to damage nucleic acids in various ways. Guanine, among the four canonical nucleobases, is particularly susceptible to oxidation, leading to the formation of oxidative lesions such as 8-oxoguanine, spiroiminodihydantoin, and guanidinohydantoin. In this study, we now report an abasic (AP) site generation from guanine residue oxidation based on photocatalytic reactions. The study

used Dickerson–Drew dodecamer DNA as the model oligo DNA for photocatalytic reactions, and the reactions were analyzed using denaturing polyacrylamide gel electrophoresis and matrix-assisted laser desorption ionization time-of-flight mass spectrometry measurements. It was observed that guanine residues are converted into AP sites by reacting with singlet oxygen generated from the photocatalyst. Guanine residues with high solvent accessibility were found to be particularly reactive with singlet oxygen. The study further proposes a mechanism for AP site generation, suggesting that further oxidation of 8-peroxy intermediate (8-OOH-G) with singlet oxygen is a crucial step in the process. These findings are important for the design and development of photocatalyst-modified functional oligo probes and the understanding of their reactions.

INTRODUCTION

Chemical modification of oligonucleotides (ONs) has enabled the creation of artificial nucleic acids with diverse properties and functions. Among them, functional ONs conjugated with photoresponsive molecules exhibit intriguing functions such as photoreaction (1–4), photo-induced electron transfer (5, 6), energy transfer (7–9), and singlet oxygen generation (10–12) in a spatiotemporal-controlled manner. Despite the numerous successful applications of photoresponsive ONs, it is also well-known that nucleic acids can suffer considerable photodamage depending on the wavelength of the irradiated light and the characteristics of the coexisting or modifying functional molecules (13–16). These lesions can hinder or impair the functionality of photoresponsive ONs. Therefore, it is essential to gain a thorough understanding of the types of lesions that can occur and the conditions under which they arise.

When focusing on photooxidation lesions among many photo-induced damages, there is no doubt that guanine, which has the lowest redox potential (1.29 V) among the four canonical nucleobases, is one of the most susceptible to oxidative lesion formation (17). Photooxidation of guanine, mediated by exogenous or endogenous photosensitizers, has been extensively studied over the past several decades owing to the structural diversity and biological significance of the resulting lesions (Fig. 1A). Representative guanine oxidation lesions include 8-oxoguanine (8-oxoG) (18–21), spiroiminodihydantoin (Sp) (22), guanidinohydantoin (Gh) (23), dehydroguanidinohydantoin (DGh) (24), imidazolone (Iz), and its hydrolysis product oxazolone (18, 25). Type I oxidation, involving hydroxyl radicals derived from photosensitizers, generates 8-oxoG and Iz, while type II oxidation, involving singlet oxygen, primarily leads to

the formation of Sp and Gh. DGh is predominantly formed via further oxidation of 8-oxoG. Additionally, 8-oxoG can also be the main product of type II oxidation in the presence of reducing agents such as glutathione (21). Lesion formation based on photo-induced electron transfer can also arise when the proximity effect occurs between the photosensitizer and the nucleic acid (26, 27). Some oxidized nucleobases can form inter- or intra-strand crosslinks through oxidative processes (28–30), and similar lesions may also be generated by photooxidation. Although some oxidative lesions have been detected in vivo and possess high mutagenicity, repair enzymes primarily excise and remove these lesions (31–33). These repair pathways minimize the risk of diseases associated with the formation of guanine oxidation lesions.

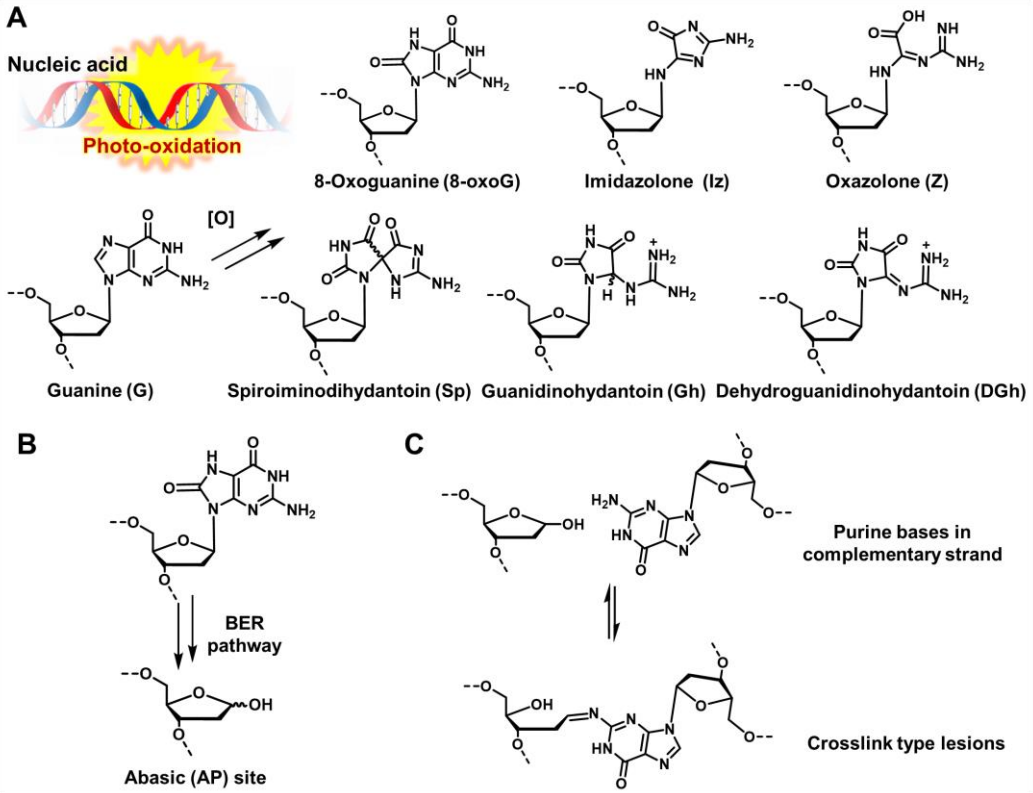

Figure 1. Oxidative lesions. (A) Representative oxidative lesions of guanine. (B) Enzymatic generation of abasic (AP) sites. (C) Representative crosslink lesions formed from AP sites.

Abasic (AP) sites are a distinct class of lesions owing to their high genotoxicity (34, 35). They arise from the hydrolysis of *N*-glycosidic bonds in purine nucleotides under acidic conditions or via enzymatic reactions in the base excision repair (BER) pathway (Fig. 1B) (36–38). Notably, AP sites can form crosslinking structures by reacting with exocyclic amino groups of purine bases in complementary DNA strands (Fig. 1C) (39, 40) or amino acid residues in proteins (41,

42). Moreover, AP sites serve as scaffolds for introducing functional molecules into nucleic acids (43–46) and crosslinking duplexes (47, 48). Recent research has focused on developing innovative methodologies for recognizing (49, 50), reacting (51), or sequencing (52) AP sites containing DNA strands.

In previous work, we developed photocatalyst-tethered ON probes for photochemical labeling of nucleic acids (53). Under light irradiation in the presence of a labeling agent, the desired labeling reaction occurred. However, light irradiation in the absence of a labeling agent resulted in complex lesions, including AP sites, as a side product. While further analysis was challenging owing to the complexity of the previous system, these results prompted us to investigate the details of photo-oxidative lesions using simpler systems. In this study, we designed a simple system with self-complementary oligo DNA duplex and used denaturing polyacrylamide gel electrophoresis (PAGE) and matrix-assisted laser desorption ionization time-of-flight mass spectrometry (MALDI–TOF MS) to analyze photocatalytic oxidative damages on DNA duplex. Notably, we found that oligo DNA undergoes photo-oxidative depurination of guanines to generate AP sites as one of the major lesions when irradiated with light in the presence of a photocatalyst such as Rose Bengal.

MATERIALS AND METHODS

General chemicals were purchased from Fujifilm Wako Pure Chemical, Tokyo Chemical Industry, Kanto Chemical, Aldrich, or Nacalai Tesque. Target DNA and RNA sequences were obtained from JBioS (Japan). MALDI–TOF MS analysis was performed using a Bruker autoflex speed instrument. Lyophilization was performed using a LABCONCO FreeZone 2.5.

Photoreaction for denaturing polyacrylamide gel electrophoresis analysis

Aliquots (2 μL) of DNA duplex (50 μM), photocatalyst (Rose Bengal, EosinY, or Ruthenium tris(bipyridine) complex) (50 μM), phosphate buffer (20 mM, pH 7.0), NaCl (100 mM), and 10% DMSO were prepared. For the photoreaction, these aliquots in 0.5 mL tubes were irradiated with 540, 505, or 455 nm light by Twin LED Light (Relyon, for RB at 540 nm 37.0 ± 7.0 mW cm^{-2}) at 0°C. The distance between the lamp and the sample was 30 mm. After irradiation for varying durations (0–5 min), loading buffer (2.0 μL, 95% formamide, 50 mM ethylenediaminetetraacetic acid (EDTA) pH 8.0) was added to the mixtures. PAGE was

performed using a 16% acrylamide gel containing 6.0 M urea, 20% formamide, and 1× TBE at 250 V for 120 min. The gel was stained with SYBR gold, and the ODNs were visualized using an FLA-5100 (Fujifilm Co.) and a ChemiDoc™ Touch Imaging System (Bio-Rad).

Photoreaction for MALDI–TOF MS analysis

Aliquots (20 μL) of DNA duplexes or G4 DNA (50 μM), photocatalyst (Rose Bengal, Eosin Y, or Ruthenium tris(bipyridine) complex) (50 μM), phosphate buffer (20 mM, pH 5.8–7.0), NaCl or KCl (100 mM), and 10% DMSO were prepared. For the photoreaction, the aliquot was divided into 10 tubes, with 2 μL of solution added to each tube. The tubes were then irradiated with 540, 505, or 455 nm light by Twin LED Light (Relyon, for RB at 540 nm 37.0 ± 7.0 mW cm^{-2}) at 0°C. The distance between the lamp and the sample was 30 mm. The irradiated aliquots in the 10 tubes were combined, and double-distilled water (dd-H_2O) (80 μL) was added. Prior to MALDI–TOF MS measurements, this 100 μL aliquot was purified using a NAP™-5 column (Cytiva) and desalted with a Sep-Pak C18 Plus short cartridge (Waters™) followed by lyophilization. The dry compound was dissolved in dd-H_2O (10 μL) and passed through a Zip-Tip® pipette tip (Millipore) to prepare the DNA sample. The MALDI–TOF MS spectrometry matrix was prepared by mixing di-ammonium hydrogen citrate (5 mg/50 μL) in H_2O and 3-hydroxypicolinic acid (25 mg/500 μL) in 1:1 H_2O:CH_3CN (v/v). A matrix (1 μL) was spotted on a MALDI–TOF MS sample plate, and a DNA sample (1 μL) was applied on top of the matrix. The samples were dried at room temperature and analyzed by MALDI–TOF MS.

APE1 treatment and purification of photoirradiated aliquot

The irradiated and collected duplex DNA aliquot (2 μL × 10 tubes) was prepared using the same procedure as described above, and dd-H_2O (80 μL) was added. This 100 μL aliquot was purified using a NAP™-5 column and lyophilized. The dry compound was dissolved in dd-H_2O (80 μL), 10× NEB buffer (10 μL), and APE1 (10 units/μL) (10 μL) were added. This solution was incubated at 37°C for 6 h and at 65°C for 20 min. It was then purified and desalted using a NAP™-5 column, Sep-Pak C18 Plus short cartridge, and Zip-Tip® pipette tip in the same manner as above. The purified sample was subsequently analyzed by MALDI–TOF MS.

Hot piperidine treatment and purification of photoirradiated aliquots

The irradiated and collected duplex DNA aliquot (2 μL × 10 tubes) was prepared using the same procedure as described above. Aqueous solution of piperidine (2 M) and β-mercaptoethanol (BME, 0.5 M) (20 μL) was added to the aliquot. This mixed solution was incubated at 90°C for 5–30 min, and dd-H_2O (60 μL) was added. This 100 μL solution was purified and desalted using a NAP^{TM}-5 column, Sep-Pak C18 Plus short cartridge, and Zip-Tip$^{®}$ pipette tip in the same manner as above. The purified sample was subsequently analyzed by MALDI–TOF MS.

RESULTS AND DISCUSSION

Discovery of AP site generation in Dickerson–Drew dodecamer DNA (DD–DNA) under photocatalytic reactions

First, we evaluated DNA damage under photocatalytic reactions using a simplified system. For this purpose, DD–DNA, a self-complementary DNA oligomer whose crystal structure has been elucidated and that forms a typical B-type duplex (54), was selected as a model sequence. In the presence of free photocatalysts such as Ruthenium tris(bipyridine) complex (Ru complex), Eosin Y (ESY), or Rose Bengal (RB), DD–DNA was exposed to light with a wavelength close to the absorption maximum of each photocatalyst: 455, 505, or 540 nm (Fig. S1). The irradiated aliquots were then analyzed by denaturing polyacrylamide gel electrophoresis (PAGE). Notably, 120 s of irradiation resulted in the near-complete disappearance of the starting DD–DNA band. In its place, two groups of bands with different mobilities compared to DD–DNA (oxidative lesions 1 and 2) were generated. Similar gel profiles were obtained regardless of the photocatalyst used (Fig. 2). Because RB exhibited the highest reactivity, we decided to use the DD–DNA and RB combination for further analysis of the reaction.

To characterize the oxidative lesions in detail, MALDI–TOF MS analysis was performed. After the photocatalytic reaction, aliquots of DD–DNA were purified, desalted, and subjected to analysis. MALDI–TOF MS analysis of an aliquot of DD–DNA after 120 s of irradiation provided valuable insights into the lesions generated (Fig. 3). The peak corresponding to intact DD–DNA (Calcd. $[M–H]^-$ 3643.6) was absent from the MS spectrum (Fig. 3B), indicating near-complete consumption, consistent with the results obtained from denaturing PAGE. In its place, peaks corresponding to DD–DNA containing guanine lesions such as Gh and/or Sp shown in Fig. 3A

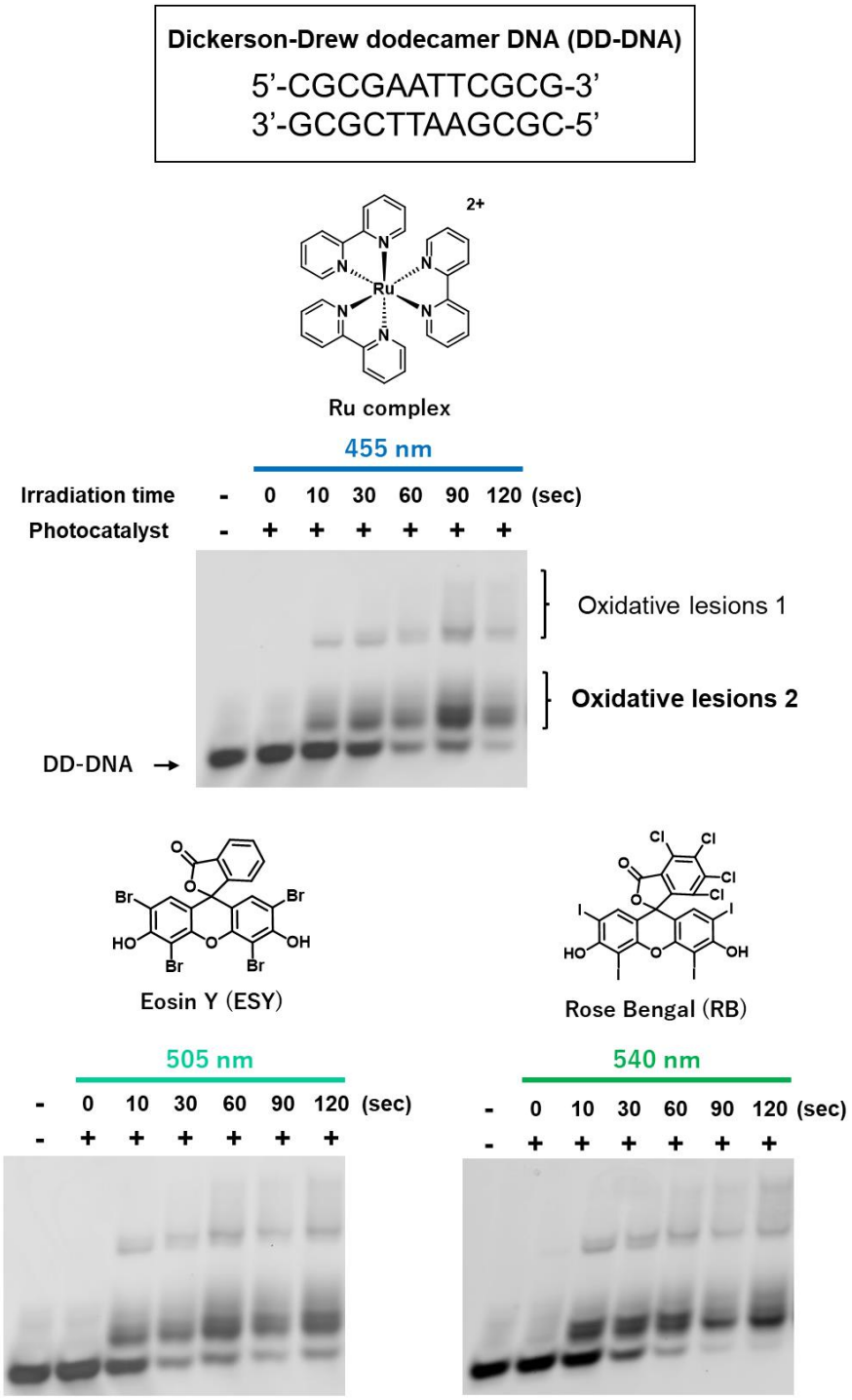

Figure 2. Denaturing polyacrylamide gel electrophoresis (PAGE) analysis of photocatalytic reactions with DD–DNA. Photocatalytic reactions were performed with 100 μM DD–DNA (50 μM duplex) and 50 μM photocatalyst in a 20 mM phosphate buffer (pH 7.0) containing 100 mM NaCl and 10% DMSO at 0°C. Each aliquot was irradiated with LED light corresponding to the absorption wavelength of each photocatalyst (455, 505, or 540 nm) for varying durations (0–120 s). The gel was stained with SYBR gold. After irradiation, two types of slower-mobility bands (oxidative lesions 1 and 2) were observed on the gel, and similar band profiles were observed for all photocatalysts.

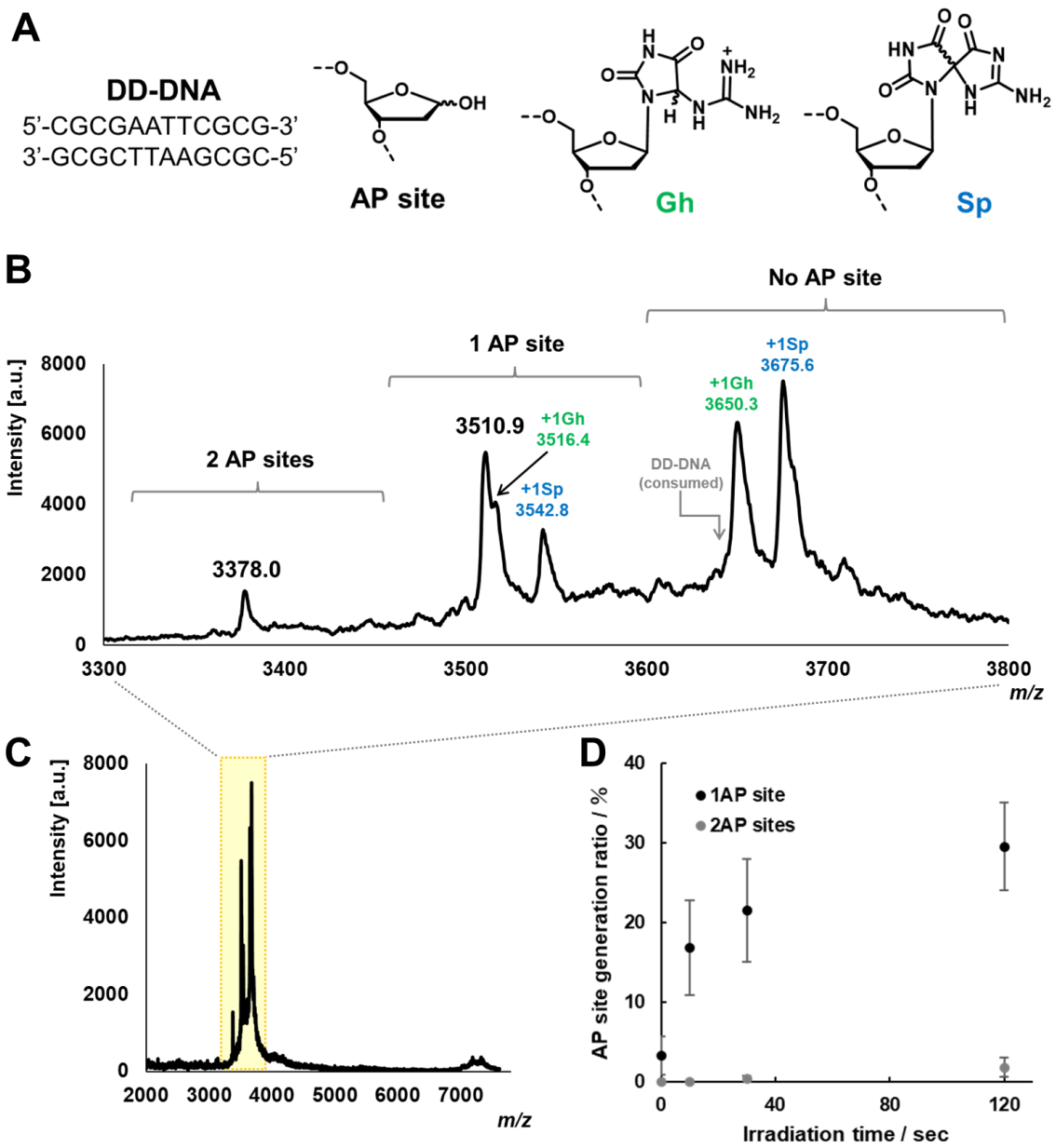

Figure 3. MALDI–TOF MS analysis of photocatalytic reactions with DD–DNA and Rose Bengal (RB). (A) DD–DNA sequence used in the experiment and representative lesions observed in MALDI–TOF MS analysis. (B, C) MALDI–TOF MS spectra after 540 nm LED light irradiation for 120 s. DD–DNA containing AP sites and/or guanine lesions such as Gh and Sp were detected as major peaks. (D) Time course of AP site generation in DD–DNA under photocatalytic reaction conditions. The generation ratio was calculated from the peak areas in the MALDI–TOF MS spectra (see supporting information for details). Photocatalytic reactions were performed with 100 μM DD–DNA (50 μM duplex) and 50 μM RB in a 20 mM phosphate buffer (pH 7.0) containing 100 mM NaCl and 10% DMSO at 0°C. Aliquots were irradiated with 540 nm LED light for varying durations (0–120 s).

converted to AP sites were detected as major peaks, suggesting that guanine residues in DD–DNA undergo not only established types of oxidation but also considerable depurination

leading to AP site formation under photocatalytic reaction conditions. These main products likely correspond to the major bands observed in the PAGE analysis (oxidative lesions 2 in Fig. 2). In contrast, the product corresponding to the gel band with the lowest mobility (oxidative lesions 1 in Fig. 2) is hypothesized to be cross-linked DD–DNA owing to the considerable band shift observed. This cross-linked DD–DNA may arise from the reaction between a G lesion or AP site and an exocyclic amino group of a guanine residue in the complementary strand (39, 40). Additionally, no band shift downstream from DD–DNA was observed on PAGE, and no peaks with a smaller mass-to-charge ratio than AP sites containing DD–DNA were detected on the MALDI–TOF MS chart (Fig. 3C). This suggests that double-strand breaks or strand cleavage mediated by AP sites are not major reactions in this system.

To quantitatively assess AP site generation under photocatalytic reaction conditions, we calculated the AP site generation ratio from MALDI–TOF MS analysis. The substantial reduction in MS value of DD–DNA upon depurination of guanine enabled us to differentiate between DD–DNA species containing no AP sites, 1 AP site, and 2 AP sites. The ratio of AP site generation in DD-DNA was calculated by dividing the sum of peak areas assigned to sequences containing AP sites by the sum of all detectable peak areas in the *m/z* value range from 3350 to 3800. The validity of quantifying the AP site generation ratio by peak area was confirmed through MALDI–TOF MS measurements of samples containing specific ratios of DD–DNA and DD–DNA–dS, where the terminal G in the DD–DNA sequence was replaced with an AP site-like spacer (see Figs. S2 and S3 for details).

The AP site generation ratio for each irradiation time was calculated from the MALDI–TOF MS spectra (including Figs. 3B and S5) obtained from three independent photocatalytic reaction experiments. The average values are shown in Fig. 3D. Before irradiation, the AP site generation ratio was 4% (Fig. 3D, 0 s), suggesting that AP sites were generated at a certain level by laser irradiation during the MALDI–TOF MS measurement. After 120 s of irradiation, the 1 AP site and 2 AP site generation ratios were 30% and 1%, respectively. The AP site generation ratio increased with increasing irradiation time (Fig. 3D, 10–120 s), confirming that AP sites were indeed generated by the photocatalytic reaction. When DD–DNA was irradiated with 455 or 505 nm light for 120 s in the presence of Ru complex or ESY, respectively, and analyzed by MALDI–TOF MS, similar MS profiles to those obtained with RB were observed (Fig. S4), indicating similar lesion generation with all three photocatalysts.

We also investigated the pH dependence of the AP site and lesion generation (Fig. S6). DD–DNA was irradiated for 120 s in the presence of RB in buffers ranging from pH 6.0–8.0, and the irradiated aliquots were analyzed by MALDI–TOF MS. Experiments at pH 6.0 yielded Gh-containing DD–DNA as a major peak and Sp-containing DD–DNA as a minor peak, whereas experiments at pH 8.0 gave Sp-containing DD–DNA as a major peak. This result is consistent with previous studies demonstrating that Gh lesion formation is favored under acidic conditions, while the Sp lesion predominates at higher pH values (55), supporting the validity of our lesion assignments. Notably, the AP site generation ratio remained relatively constant across the pH range studied.

Position of AP site generation in the DD–DNA based on photocatalytic reactions

Next, the position of AP site generation in DD–DNA was investigated. For this, the enzyme apurinic/apyrimidinic endonuclease 1 (APE1), which cleaves duplex DNA at AP site positions, generating fragments with a 3′-terminal hydroxyl group, was used (56). In this experiment, DD–DNA was exposed to 540 nm light for 10 and 120 s in the presence of RB. The irradiated samples were then treated with APE1 for 6 h, purified, and analyzed by MALDI–TOF MS. In addition to uncleaved DD–DNA without AP sites, several cleaved DNA fragments were observed in the MS spectrum of the 10 s irradiated aliquot (Fig. 4). The DNA fragment **5′-CGCGAATTCGC-3′** (calcd. $[M–H]^-$ 3314.5) was predominantly observed. The minor peaks correspond to fragments cleaved at other G residues: **5′-CGAATTCGCG-3′** (calculated $[M–H]^-$ 3025.5) and **5′-CGCGAATTC-3′** or **5′-CGAATTCGC-3′** (calcd. $[M–H]^-$ 2696.5). These results suggest that AP sites in DD–DNA are primarily generated by depurination of the terminal G. In contrast, the MS spectrum of the 120 s irradiated aliquot exhibited complex peaks, and some damaged sequences, including AP sites, were not cleaved (Fig. S7). This observation implies that the extensive formation of AP sites, Sp, and Gh lesions alters the duplex structure of DD–DNA, hindering APE1 recognition.

As an alternative method to identify the positions of oxidized guanine lesions, including AP sites, in DD–DNA, we used hot piperidine treatment. Oxidized guanine lesions undergo depurination upon treatment with hot piperidine, resulting in strand cleavage via the formation of a Schiff base intermediate (57) (Fig. S8). The rate of this cleavage reaction is known to vary depending on the type of oxidized guanine lesion, with AP sites being cleaved

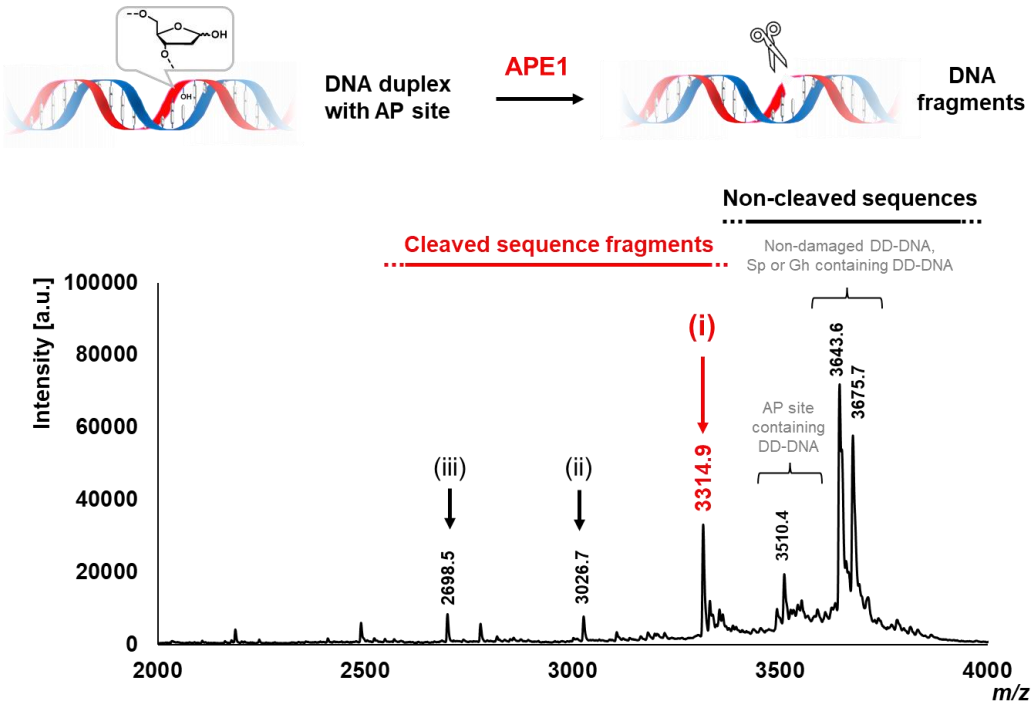

	Found (*m/z*)	Speculated Sequence	Calcd. [M-H]$^-$
DD-DNA	3643.6	5'-CGCGAATTCGCG-3'	3643.6
Major cleaved fragment (i)	**3314.9**	5'-CGCGAATTCGC-3'	**3314.5**
Minor cleaved fragment (ii)	3026.7	5'-CGAATTCGCG-3'	3025.5
Minor cleaved fragment (iii)	2698.5	5'-CGCGAATTC-3' 5'-CGAATTCGC-3'	2696.5

Figure 4. Positions of AP sites generated in DD–DNA by photocatalytic reaction. Photocatalytic reactions were performed with 100 µM DD–DNA (50 µM duplex) and 50 µM RB in a 20 mM phosphate buffer (pH 7.0) containing 100 mM NaCl and 10% DMSO at 0°C. Aliquots were irradiated with 540 nm LED light for 10 s, treated with APE1 (1 unit/µL) in 1× NEB buffer at 37°C for 6 h, and finally analyzed by MALDI-TOF MS.

more rapidly than other lesions. In other words, short-term hot piperidine treatment is expected to provide information primarily on the position of AP sites. Specifically, aqueous piperidine (1 M) and 2-mercaptoethanol (BME) (0.25 M) were directly added to the aliquot after 120 s of light irradiation, followed by incubation at 90°C and analysis by MALDI–TOF MS. The MS spectrum obtained after 1 min of hot piperidine treatment revealed peaks corresponding to uncleaved AP sites, Gh, and/or Sp-containing DD–DNA, indicating that the incubation time was insufficient (Fig. S9). On the one hand, after 5 min of hot piperidine treatment, only a minor uncleaved peak was observed for the AP site-containing DD–DNA, suggesting that most of it had been cleaved (Fig. S9). On the other hand, the DD–DNA containing Gh or Sp lesion still showed a clear peak because these lesions have been reported

to be relatively slow in hot piperidine-mediated cleavage reactions (57). Focusing on the cleavage fragments, the major fragment peak corresponded to **5′-CGCGAATTCGCp-3′** (calcd. $[M–H]^-$ 3394.5). This result indicates that the AP sites are primarily derived from terminal G, which aligns well with the results obtained from APE1 treatment. A minor peak assignable to **5′-CGCGAATTCp-3′** (calcd. $[M–H]^-$ 2776.4) or **5′-pCGAATTCGCp-3′** (calcd. $[M–H]^-$ 2856.4) was also detected, suggesting that extended irradiation time enables the conversion of internal G to AP sites. Additionally, fragments with other guanine lesions, such as **5′-pCGAATTCGC-*Gh*-3′** (calcd. $[M–H]^-$ 3112.5) and **5′-pCGAATTCGC-*Sp*-3′** (calcd. $[M–H]^-$ 3137.5), were also present among the minor peaks. No fragments containing an intact terminal G were detected. When the incubation time was extended to 10, 30, and 60 min, the peak corresponding to DD–DNA containing Gh lesions nearly disappeared, and the peak of DD–DNA containing Sp lesions became smaller than the main fragment peak, indicating that these lesion-containing DD–DNAs were also cleaved (Fig. S10). The major fragment under these conditions was also **5′-CGCGAATTCGCp-3′**. These results underscore that not only AP sites but also Gh and Sp lesions are generated primarily from terminal G.

Identification of reactive oxygen species that mainly contribute AP site generation in DD–DNA by photocatalytic reactions

In general, oxidation reactions initiated by photocatalysis can be classified into two types: type I oxidation, which involves hydroxyl radicals, and type II oxidation, which involves singlet oxygen (Fig. 5A). It is also conceivable that other secondarily generated reactive oxygen species may contribute to AP site formation. To determine which reactive oxygen species are primarily responsible for the generation of AP sites in DD–DNA, we performed photocatalytic reactions in the presence of mannitol, a hydroxyl radical scavenger, or NaN_3, a singlet oxygen scavenger, and compared the AP site generation ratios (58–60). While the AP site generation ratio calculated from the MALDI–TOF MS spectra was not considerably reduced in the presence of mannitol (Fig. 5B and Fig. S11), AP site generation was markedly suppressed in the presence of NaN_3, and the ratio was comparable to that before irradiation. An aliquot of DD–DNA following the photocatalytic reaction in the presence of NaN_3 and mannitol was also analyzed by denaturing PAGE. The results demonstrated that the shifted bands observed in

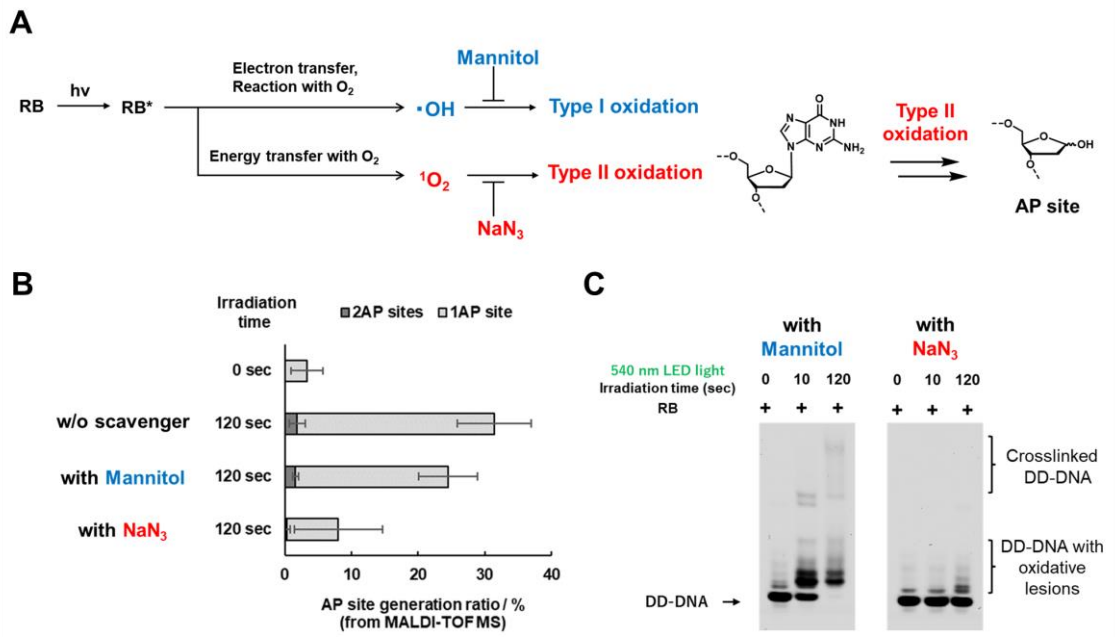

Figure 5. Identification of reactive oxygen species that primarily contribute to AP site generation in DD–DNA under photocatalytic conditions. (A) Schematic representations of type I and type II oxidation, along with their corresponding scavengers. (B) AP site generation ratio in DD–DNA in the presence of each scavenger. The generation ratio was calculated based on peak areas in the MALDI–TOF MS spectra. (C) Denaturing PAGE analysis of photocatalytic reactions in the presence of each scavenger. Photocatalytic reactions were performed with 100 μM DD–DNA (50 μM duplex), 50 mM of each scavenger (NaN_3 or mannitol), and 50 μM RB in a 20 mM phosphate buffer (pH 7.0) containing 100 mM NaCl at 0°C. Aliquots were irradiated with 540 nm LED light for 120 s.

the absence of NaN_3 were nearly absent in the presence of NaN_3 (Fig. 5C). This contrasts with mannitol, which exhibited a gel profile similar to that of the system without a scavenger (Fig. 2). Moreover, the addition of another singlet oxygen scavenger, 1,4-diazabicyclo[2.2.2]octane (DABCO) (61), also reduced the AP site generation ratio to trace levels (Fig. S11. Conversely, the addition of catalase or superoxide dismutase (SOD), which scavenge hydrogen peroxide or superoxide anion (62) respectively, did not considerably suppress AP site generation (Fig. S11), confirming that these other reactive oxygen species do not play a major role in the photocatalytic AP site generation observed here.

AP sites were also generated when DD–DNA was incubated with an endoperoxide (EP) reagent (63), which quantitatively generates singlet oxygen upon heating at 35°C (Fig. S12). Notably, this reaction was found to be more efficient in a deuterated buffer, which prolongs the lifetime of singlet oxygen (10, 61). These observations further support the notion that AP sites are primarily generated via type II oxidation. Considering the results on the position of AP sites,

AP site generation in DD–DNA is thought to occur mainly through the reaction of highly solvent-accessible G residues, such as the terminal G, with singlet oxygen produced by the photocatalyst. Conversion of the terminal G to an AP site, Gh, or Sp lesion by initial irradiation changes the base-pairing stability (64) and can increase the solvent accessibility of internal Gs, allowing extended irradiation to generate additional lesions at these internal sites (Fig. S13).

Possible mechanisms for AP site generation under the photocatalytic reaction

To investigate the mechanism of AP site generation in greater detail, we endeavored to elucidate the mechanism at the molecular level. To our knowledge, there is no detailed report on the mechanism of AP site generation via photocatalytic reactions. However, G lesions such as Gh and Sp have been extensively studied using G monomers and oligomers, and the generation mechanism of these lesions based on the reaction with singlet oxygen has been well-established (19, 55, 65). According to previous studies, G primarily undergoes a Diels–Alder reaction with singlet oxygen to produce intermediate **1**. The cleavage of the C–O bond in intermediate **1** leads to the formation of 8-peroxy intermediate **2** (55). Owing to its high reactivity, intermediate **2** is dehydrated to form intermediate **3** (Fig. 6 pathway a), which then interacts with water to yield intermediate **4** (55). The subsequent addition of water and

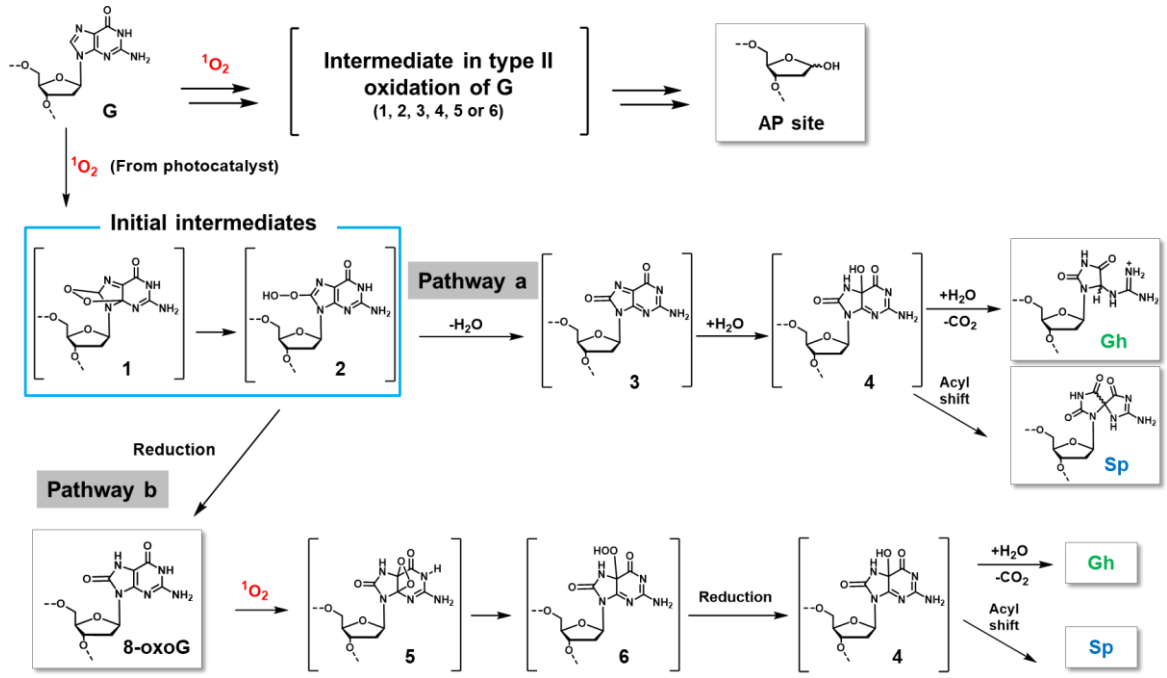

Figure 6. Lesions and AP site generation via type II oxidation of guanine residues. The pathways for Gh and Sp generation from G have been previously reported, involving intermediates 1–6.

decarboxylation of intermediate **4** results in the production of Gh, while acyl transition leads to Sp generation. Alternatively, intermediate **2** can be directly reduced to form 8-oxoG (Fig. 6 pathway b). Furthermore, the reaction of 8-oxoG with another singlet oxygen molecule also yields **4** through highly reactive intermediates **5** and **6,** resulting in the formation of Sp and Gh (19, 65). In the photocatalytic reaction involving DD–DNA, there was no significant generation of AP sites based on the elimination of nucleobases other than G. Therefore, it is highly likely that the pathway for AP site generation shares partial commonality with the generation of G lesions and branches from any of the type II oxidation intermediates **1–6**.

While it is extremely challenging to fully determine the specific intermediate from which the AP site is generated, examining the role of 8-oxoG in the primary pathway for photocatalytic AP site generation in DD–DNA could yield important mechanistic insights. The MALDI–TOF MS chart in Fig. 3 shows no peaks corresponding to 8-oxoG-containing DD–DNA after 120 s of photoirradiation with 540 nm light. However, after irradiating DD–DNA for just 10 s in the presence of 5 μM RB, a peak associated with 8-oxoG-containing DD–DNA was detected (Fig. S14). Additionally, this peak vanished after 300 s of irradiation, and in its place, peaks corresponding to DD–DNA containing Gh, Sp, or AP sites emerged. These findings suggest that 8-oxoG contributes to the formation of at least one of these lesions in this system.

Motivated by this result, we developed the DD–DNA-8-oxoG (Fig. 7A), wherein the terminal G residue of the DD–DNA sequence is replaced by 8-oxoG. If AP sites are primarily produced from intermediates **5** and **6** in pathway b, then the AP site generation ratio for DD–DNA-8-oxoG, which bypasses the initial reaction step with singlet oxygen, should be considerably higher than that of DD–DNA. Conversely, if AP sites arise from initial intermediates **1**, **2**, or **3**, substituting 8-oxoG for terminal G should lead to a substantial decrease in the AP site generation ratio. In the presence of RB, DD–DNA-8-oxoG was irradiated with 540 nm light for either 10 or 120 s, desalted, purified, and analyzed using MALDI–TOF MS. The results indicated that the intact DD–DNA-8-oxoG peak nearly vanished after 10 s of irradiation; however, peaks associated with AP sites were not detected as main peaks, and substantial AP site generation could not be confirmed. Instead, the terminal 8-oxoG was quickly transformed into lesions such as Gh and Sp (Fig. 7B). Previous studies have noted that intermediate **6** can also transform into the DGh lesion, and its mass spectrum is very similar to that of Gh (24), suggesting that some main peaks may contain DGh rather than Gh. Alongside these major peaks, several minor

peaks were also identified. These may represent damaged DD–DNA-8-oxoG related to the imidazolone (Iz) lesion and its hydrolysate, which have similarly been documented in the reactions of 8-oxoG with singlet oxygen (66). This result clearly demonstrates that 8-oxoG and the downstream intermediates **4**, **5**, or **6** are not part of the main pathway for AP site generation. Furthermore, while the multi-step hydrolysis of Iz lesions can also lead to the formation of AP sites (67), the considerable reduction in AP site generation rates following 8-oxoG substitution implies that Iz-derived AP site generation is not the primary mechanism in this system either. Extended irradiation time resulted in considerable AP site generation; however, the main peaks in the mass spectrometry chart included both Gh/Sp lesions and AP

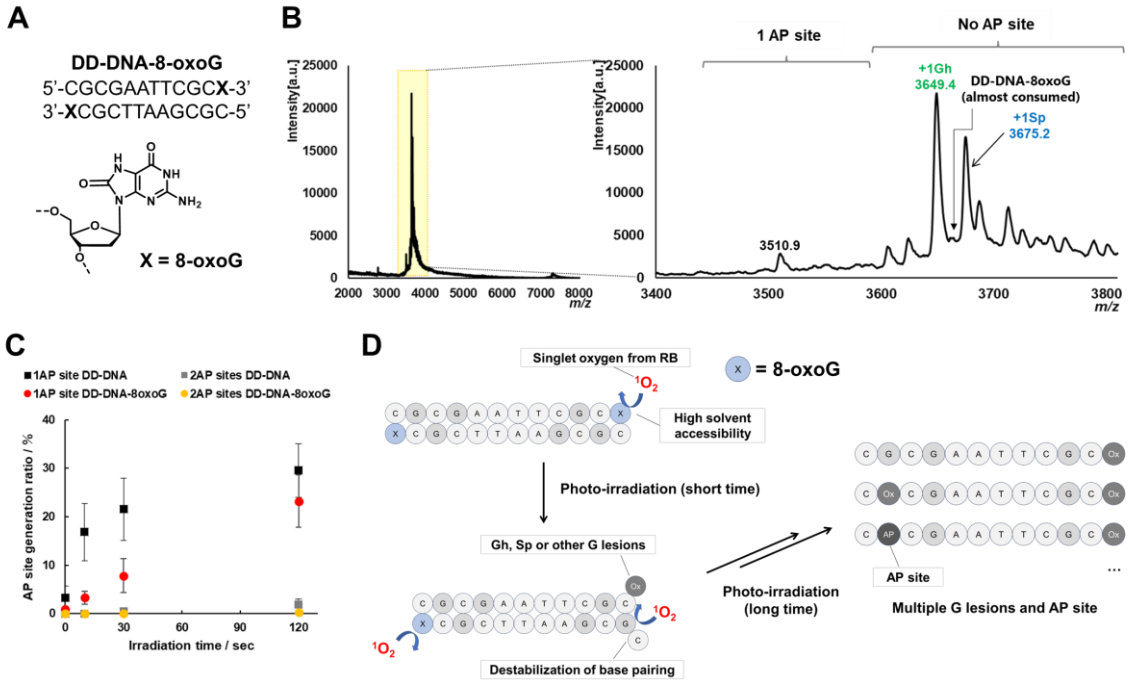

Figure 7. Photocatalytic reaction involving 8-oxoG modified DD–DNA (DD–DNA-8-oxoG) and Rose Bengal. (A) The sequence of DD–DNA-8-oxoG used in the experiment. (B) MALDI–TOF MS chart obtained after 10 s of irradiation with a 540 nm LED light. The photocatalytic reactions were performed with 100 μM DD–DNA-8-oxoG (50 μM duplex) and 50 μM photocatalyst in a 20 mM phosphate buffer (pH 7.0) containing 100 mM NaCl at 0°C. DD–DNA-8-oxoG featuring Gh and Sp was identified as the main peaks, while AP site generation was minimal. (C) The time course of AP site generation in DD–DNA-8-oxoG during the photocatalytic reaction. The generation ratio was determined from the peaks in the MALDI–TOF MS chart. The ratio and rate of AP site formation in DD–DNA-8-oxoG were considerably lower compared to those in unmodified DD–DNA. (D) Proposed mechanism for oxidative lesions and AP site formation in DD–DNA-8-oxoG. The conversion of the terminal 8-oxoG to an oxidative lesion may enhance the solvent accessibility of the internal G, facilitating the generation of additional AP sites and G lesion formation.

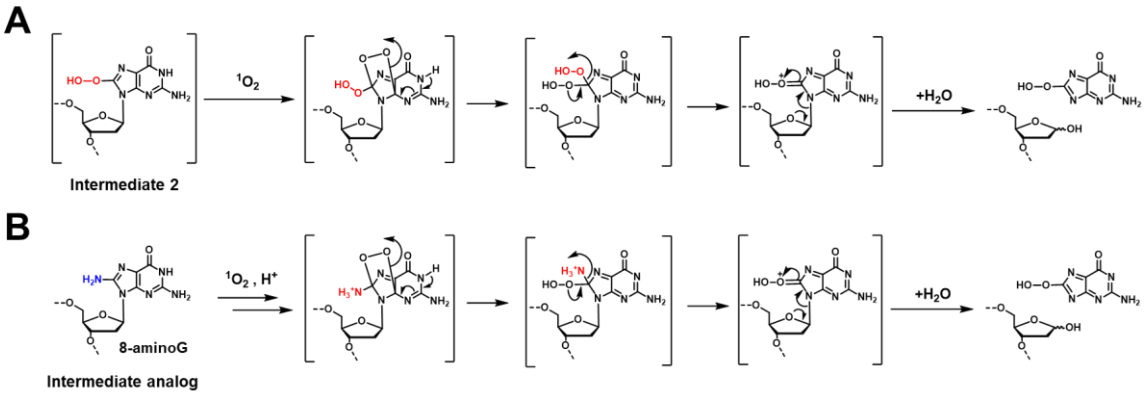

Figure 8. The suggested reaction mechanisms for the generation of AP sites through photocatalytic reactions, using 8-aminoG as an intermediate analog to validate this proposed mechanism. (A) The interaction of peroxide intermediate 2 with singlet oxygen can produce a more reactive intermediate, resulting in rapid depurination. (B) The reaction between singlet oxygen and 8-aminoG under weakly acidic conditions, followed by the protonation of the aliphatic amino group, is expected to facilitate the formation of intermediates similar to the proposed reaction mechanism, thereby inducing a depurination reaction.

sites (Figs. 7C and S15). It is likely that the destabilization of the terminal base pairing owing to the transformation of the terminal 8-oxoG lesion allows singlet oxygen to access the internal G, leading to further AP site generation (Fig. 7D). These findings suggest that AP site generation mainly occurs from the reaction of the initial intermediates **1** or **2** with singlet oxygen during type II oxidation.

The direct depurination reactions of Diels–Alder intermediate **1** and 8-peroxy intermediate **2** (Fig. S16) represent potential mechanisms for AP site generation that may compete with the formation of the downstream intermediates depicted in Fig. 7. Conversely, 8-peroxy intermediate **2** has the capacity to react with additional singlet oxygen, potentially yielding a more reactive intermediate. Depurination from this intermediate could also be a viable mechanism for AP site generation (Fig. 8A). To explore this possibility, we endeavored to design an analog of the peroxide intermediate. A G residue modified at the 8-position with a functional group that is electron-donating and acts as a leaving group would be suitable as an analog of the peroxide intermediate, with 8-aminoG (68) fulfilling this criterion (Fig. 8B). While there are reports on the oxidation reactions of non-canonical purine bases featuring additional arylamino or alkylamino groups (69–71), the reaction of 8-aminoguanine with singlet oxygen has yet to be explored. The amino group of 8-aminoG would transition from an aromatic amine

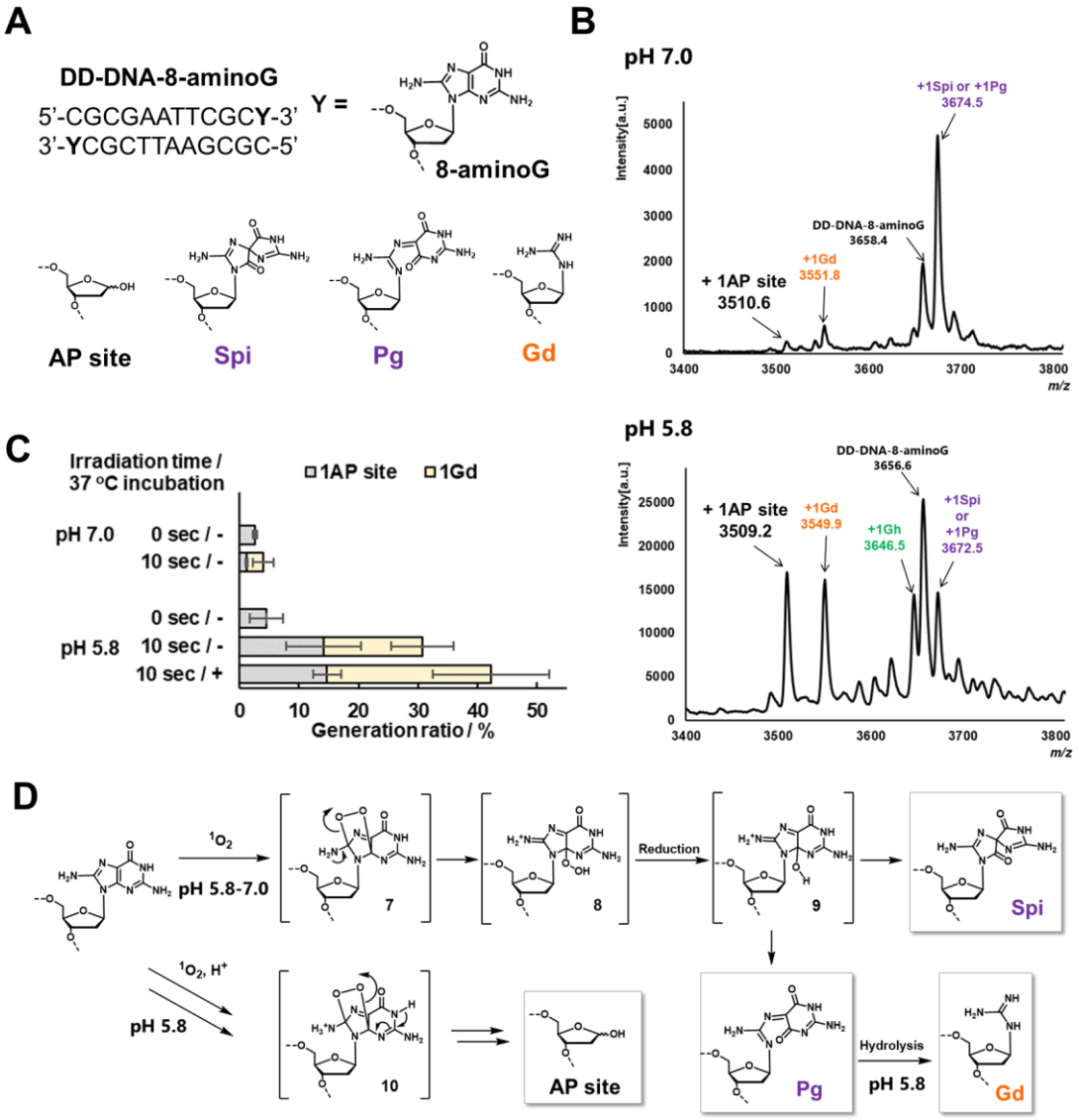

Figure 9. Photocatalytic reaction involving 8-aminoG-modified DD–DNA (DD-DNA-8-aminoG) and Rose Bengal. (A) The DD-DNA-8-aminoG sequence used in the experiment, along with the chemical structure of the AP site and the proposed structures of 8-aminoG-specific oxidation lesions (SPi, Pg, and Gd). (B) MALDI–TOF MS spectrum following 10 s of 540 nm LED light irradiation at pH 7.0 and pH 5.8. The photocatalytic reactions were performed with 100 μM DD-DNA-8-aminoG (50 μM duplex) and 50 μM photocatalyst in a 20 mM phosphate buffer (pH = 7.0 or 5.8) containing 100 mM NaCl and 10% DMSO at 0°C. (C) The ratio of AP site or Gd-containing DD-DNA-8-aminoG before and after 10 s of irradiation and subsequent incubation at 37°C for 24 h. (D) Proposed reaction mechanisms for the generation of AP sites and SPi, Pg, or Gd lesions from 8-aminoG, based on the photocatalytic reaction.

to an aliphatic amine upon the addition of singlet oxygen. Furthermore, if the photocatalytic reaction is performed under mildly acidic conditions, only the aliphatic amine can be

protonated, making it an ideal analog to replicate the proposed reaction mechanism. Guided by this prediction, we engineered DD–DNA-8-aminoG, substituting the terminal G of DD–DNA with 8-aminoG (Fig. 9A), and investigated whether the efficiency of AP site generation of DD–DNA-8-aminoG under photocatalytic conditions varied considerably at pH 7.0 and 5.8. Figure 9B shows the MS chart of DD–DNA-8-aminoG following 10 s of irradiation in the presence of RB. At pH 7.0, along with the peak for intact DD–DNA-8-aminoG, there was confirmation of a peak corresponding to the DD–DNA-8-aminoG sequence with oxidized lesions of 8-aminoG; however, no notable AP site generation was detected. Although there are no previous studies on the oxidized lesion of 8-aminoG, it is expected that the endoperoxide bridge in intermediate **7** is cleaved owing to electron donation from the amino group under neutral conditions, leading to the formation of intermediate **8** (Fig. 9D). Even if a [2+2] cycloaddition occurs instead of a [4+2] cycloaddition, the same intermediate **8** would be produced (Fig. S19A). If this highly reactive intermediate **8** undergoes reduction to yield intermediate **9**, it can either form a spiro ring or cleave the five-membered ring, resulting in the previously unreported spiroimidazolone (Spi) or pyrimidinylideneguanidine (Pg) lesion (Figs. 9A, D). Conversely, after 10 s of irradiation at pH 5.8, alongside the peaks of sequences featuring Spi and Pg lesions, peaks corresponding to sequences in which 8-aminoG converted to AP sites were also detected, confirming significant AP site generation (Figs. 9B and S17). It is worth mentioning that the photocatalytic AP site generation ratio for DD–DNA without 8-aminoG at pH 5.8 was not considerably different from that at pH 7.0 (Fig. S20). This pH-dependent AP site generation is specific to 8-aminoG. MS numbers associated with DD–DNA-8-aminoG, where 8-aminoG was converted to DGh, Gh, or an unreported guanidine (Gd) lesion, were also identified. DGh and Gh can be formed through [2+2] cycloaddition or [4+2] cycloaddition of singlet oxygen with 8-aminoG (Fig. S19B), while the Gd lesion can arise from the hydrolysis of the Pg lesion (Fig. 9D). To verify that the AP site was generated primarily through the proposed mechanism involving intermediate **10**, and not through further hydrolysis of Gd, the aliquot irradiated for 10 s at pH 5.8 was incubated at 37°C for 24 h, and the ratio of sequences containing Gd or the AP site to the total peak area was assessed. In the MS chart following incubation, the peak area of the sequence containing Gd increased, while the peak area ratio of the sequence with AP sites remained largely unchanged (Figs. 9C and S18). This finding indicates that the AP site is not produced through the hydrolysis of Gd. Collectively, these

results strongly suggest that the overoxidation of 8-peroxy intermediate **2** is one of the mechanisms responsible for the photocatalytic generation of the AP site.

AP site generation in various duplexes and G4 DNA by photocatalytic reaction

To explore the sequence dependence of AP site generation through photocatalytic reactions, we first designed a sequence where the 5′-CGCG segment of DD–DNA was changed to either CGGC or GGGG and subsequently examined the AP site generation ratio for each sequence (Figs. 10, S21 and S22). The results indicated that all sequences exhibited similar generation ratios to DD–DNA, suggesting that rearranging the sequences near the termini does not considerably impact the AP site generation ratio. Conversely, when a photoreaction was performed using a non-terminal G-C sequence—where TTT and AAA were added to both ends of DD–DNA—the AP site generation rate remained largely unchanged following photoirradiation (Figs. 10 and S23). Additionally, when G and C were added to both ends of

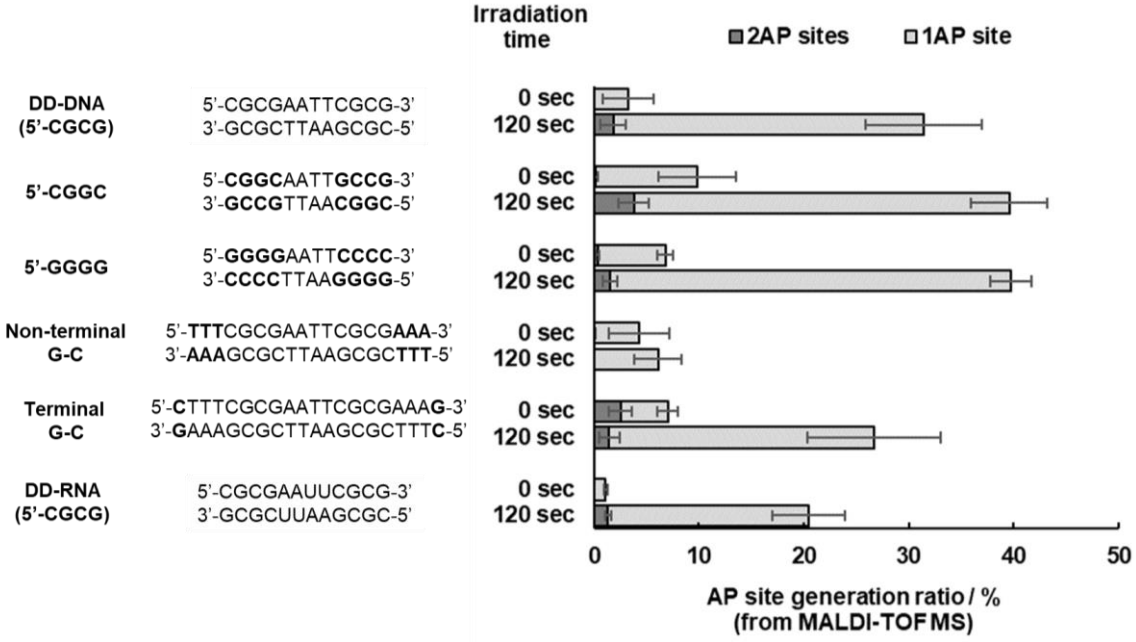

Figure 10. AP site generation ratio in various duplexes via photocatalytic reaction. The reactions were performed using a 100 μM DNA or RNA strand (50 μM duplex) and 50 μM RB in 20 mM phosphate buffer (pH 7.0) with 100 mM NaCl and 10% DMSO at 0°C. Aliquots were irradiated with 540 nm LED light.

the non-terminal G sequence, forming a terminal G–C sequence, the AP site generation ratio increased after the photoirradiation (Figs. 10 and S24). These findings further indicate that terminal G, owing to its high solvent accessibility, is crucial for effective AP site generation in duplex DNA.

Given that the glycosidic bond in RNA is stronger than that in DNA, it is assumed that depurination occurs less frequently in RNA than in DNA (72). Consequently, research on AP sites in RNA is notably limited compared to DNA (73), leaving this area largely unexplored. We investigated whether AP sites can also form in RNA under photocatalytic oxidation conditions. When we used DD–RNA, which has an RNA backbone in place of DD–DNA, the generation ratio was lower than that observed in DD–DNA; however, significant AP site generation was confirmed following light irradiation (Figs. 10 and S25). This finding suggests that AP sites can also represent a major type of lesion in RNA under photocatalytic oxidation conditions.

Finally, we investigated the potential for generating AP sites in DNA structures other than double strands under photocatalytic oxidation conditions. For this purpose, we used the human telomere (HT) G4 DNA sequence, known to form a hybrid G4 structure in the presence of K^+ and an anti-parallel G4 structure with Na^+. We performed photocatalytic reactions with each salt (Figs. S26 and S27). Notably, the generation ratio of AP sites in HT G4 DNA following the photocatalytic reaction with K^+ was found to be higher than that observed with Na^+ (Fig. S28A). Conversely, the photocatalytic generation ratio of AP sites in DD–DNA in K^+ phosphate buffer for hybrid G4 formation showed no considerable difference compared to that in the standard phosphate buffer used in this study (Figs. S29 and Fig. 3). These findings show that the increased AP site generation in HT G4 when K^+ is present is attributable to changes in the solvent accessibility of G residues owing to differences in topology, rather than the influence of the cation itself. Furthermore, this AP site generation ratio surpasses that of all duplex DNA examined to date, with a higher proportion of sequences containing multiple AP sites observed after irradiation. This indicates that certain G quartet-forming G residues, which are highly solvent-accessible, can be effectively converted to AP sites by singlet oxygen (Fig. S28B).

CONCLUSION

In this study, we discovered the phenomenon of AP site generation when DD–DNA was irradiated with light in the presence of a photocatalyst such as RB. The evaluation of AP site generation was performed by analyzing the peaks in the MALDI–TOF MS chart, allowing for a quantitative calculation of the AP site generation ratio in oligo DNA. It is important to note that not only AP sites but also other oxidative lesions, such as Gh and Sp, can be observed and easily analyzed without the need for enzymatic digestion. It was surprising to discover that the

AP site was generated at a ratio comparable to that of the well-known Gh and Sp. This comparison was primarily enabled by the MALDI–TOF MS analysis. In previous studies, oxidized DNA was typically examined only after enzymatic digestion and isolation via high-performance liquid chromatography. Consequently, this kind of AP site generation may have been overlooked in previous studies.

Treatment with APE1 and hot piperidine following the photocatalytic reaction, along with photocatalytic reactions using various duplexes, revealed that Gs with high solvent accessibility are hotspots for AP site generation. Verification with various reactive oxygen species scavengers indicated that this photocatalytic AP site generation was primarily mediated by singlet oxygen derived from the photocatalyst. Experiments involving 8-oxoG and 8-aminoG suggested that the depurination of a highly reactive intermediate, resulting from further oxidation of the 8-peroxy intermediate (8-OOH-G) with singlet oxygen is one of the potential mechanisms for AP site generation in DD–DNA. Notably, it was suggested that 8-aminoG generates AP sites in a pH-dependent manner based on a photocatalytic reaction and serves as an effective analog for mimicking the further oxidation reaction of 8-OOH-G. Additionally, AP sites were efficiently generated in the hybrid HT G4 DNA during the photocatalytic reaction. Furthermore, AP site formation occurs not only in DNA but also in RNA. Given that RNA can adopt various higher-order structures, it is likely that further hotspots may be identified in the future. When using photo-crosslinking or photo-labeling techniques on RNA, precautions should be taken to minimize the generation of AP sites owing to unintended oxidation.

Our findings shed light on the specific locations and mechanisms through which AP sites are generated via photocatalytic reactions. This knowledge will greatly assist in the design and development of photocatalyst-modified functional oligo probes that exhibit fewer side reactions, as well as enhance our understanding of their functions and interactions.

DATA AVAILABILITY

SUPPLEMENTARY DATA

Supplementary Data are available.

ACKNOWLEDGEMENTS

We thank Miyuki Aihara for assistance with sample preparation for MALDI-TOF MS analysis. We thank the Tagen Central Analytical Facility and the support program for young researchers from Tohoku University Technical Support Center for supporting MALDI-TOF MS measurement.

FUNDING

This work was supported in part by the Japan Science and Technology Agency (JST) FOREST program (No. JPMJFR2002 to K.O.); Grant-in-Aid for Scientific Research (B) (No. JP24K01641 to K.O. and No. JP23H02076 to F.N.), Scientific Research on Transformative Research Areas (A) "Biophysical Chemistry for Material Symbiosis" (No. JP23H04051 to K.O.), JSPS Fellows (No. JP22J01195 to Y.Y.), and Early-Career Scientists (No. 22K14792 to Y.Y) from the Japan Society for the Promotion of Science (JSPS); and the research program of the Crossover Alliance to Create the Future with People, Intelligence and Materials from MEXT, Japan.

Conflict of interest statement

None declared.

REFERENCES

1. Lubbe,A.S., Szymanski,W. and Feringa,B.L. (2017) Recent developments in reversible photoregulation of oligonucleotide structure and function. *Chem. Soc. Rev.*, **46**, 1052–1079.
2. Wang,C., O'Hagan,M.P., Li,Z., Zhang,J., Ma,X., Tian,H. and Willner,I. (2022) Photoresponsive DNA materials and their applications. *Chem. Soc. Rev.*, **51**, 720–760.
3. Kamiya,Y. and Asanuma,H. (2014) Light-driven DNA nanomachine with a photoresponsive molecular engine. *Acc. Chem. Res.*, **47**, 1663–1672.
4. Onizuka,K., Yamano,Y., Abdelhady,A.M. and Nagatsugi,F. (2022) Hybridization-specific chemical reactions to create interstrand crosslinking and threaded structures of nucleic acids. *Org. Biomol. Chem.*, **20**, 4699–4708.
5. Fan,S., Takada,T., Maruyama,A., Fujitsuka,M. and Kawai,K. (2023) Programmed Control of Fluorescence Blinking Patterns based on Electron Transfer in DNA. *Chem. - A Eur. J.*, **29**.
6. Onizuka,K., Ishida,K., Mano,E. and Nagatsugi,F. (2019) Alkyne-Alkyne Photo-cross-linking on the Flipping-out Field. *Org. Lett.*, **21**, 2833–2837.

7. Kashida,H., Azuma,H., Sotome,H., Miyasaka,H. and Asanuma,H. (2024) Site-Selective Photo-Crosslinking of Stilbene Pairs in a DNA Duplex Mediated by Ruthenium Photocatalyst. *Angew. Chemie - Int. Ed.*, **63**, 1–7.
8. Kato,T., Kashida,H., Kishida,H., Yada,H., Okamoto,H. and Asanuma,H. (2013) Development of a robust model system of FRET using base surrogates tethering fluorophores for strict control of their position and orientation within DNA duplex. *J. Am. Chem. Soc.*, **135**, 741–750.
9. Ensslen,P. and Wagenknecht,H.A. (2015) One-Dimensional Multichromophor Arrays Based on DNA: From Self-Assembly to Light-Harvesting. *Acc. Chem. Res.*, **48**, 2724–2733.
10. Hong,I.S. and Greenberg,M.M. (2005) DNA interstrand cross-link formation initiated by reaction between singlet oxygen and a modified nucleotide. *J. Am. Chem. Soc.*, **127**, 10510–10511.
11. Op De Beeck,M. and Madder,A. (2012) Sequence specific DNA cross-linking triggered by visible light. *J. Am. Chem. Soc.*, **134**, 10737–10740.
12. Schmidt,M.J. and Summerer,D. (2013) Red-light-controlled protein-RNA crosslinking with a genetically encoded furan. *Angew. Chemie - Int. Ed.*, **52**, 4690–4693.
13. Lord,C.J. and Ashworth,A. (2012) The DNA damage response and cancer therapy. *Nature*, **481**, 287–294.
14. Roos,W.P., Thomas,A.D. and Kaina,B. (2016) DNA damage and the balance between survival and death in cancer biology. *Nat. Rev. Cancer*, **16**, 20–33.
15. Zhao,Y., Simon,M., Seluanov,A. and Gorbunova,V. (2023) DNA damage and repair in age-related inflammation. *Nat. Rev. Immunol.*, **23**, 75–89.
16. Antusch,L., Gaß,N. and Wagenknecht,H.A. (2017) Elucidation of the Dexter-Type Energy Transfer in DNA by Thymine–Thymine Dimer Formation Using Photosensitizers as Artificial Nucleosides. *Angew. Chemie - Int. Ed.*, **56**, 1385–1389.
17. Steenken,S. and Jovanovic,S. V (1997) How Easily Oxidizable Is DNA? One-Electron Reduction Potentials of Adenosine and Guanosine Radicals in Aqueous Solution.
18. Cadet,J., Berger,M., Buchko,G.W., Joshi,P.C., Raoul,S. and Ravanat3,J.-L. (1994) 5-di-0-acetyl-2-deoxy-/S-D-eiytóro-pentofuranosyl)amino]-5-(2ti)-oxazolone: A Novel and Predominant Radical Oxidation Product of 3′,5′-Di-0-acetyl-2′-deoxyguanosine.

19. Sheu,C. and Foote,C.S. (1995) Reactivity toward Singlet Oxygen of a 7, 8-Dihydro-8-oxoguanosine ("8-Hydroxyguanosine") Formed by Photooxidation of a Guanosine Derivative. *J. Am. Chem. Soc.*, **117**, 6439–6442.
20. Ravanat,J.L. and Cadet,J. (1995) Reaction of Singlet Oxygen with 2'-Deoxyguanosine and DNA. Isolation and Characterization of the Main Oxidation Products. *Chem. Res. Toxicol.*, **8**, 379–388.
21. Ravanat,J.L., Di Mascio,P., Martinez,G.R., Medeiros,M.H.G. and Cadet,J. (2000) Singlet oxygen induces oxidation of cellular DNA. *J. Biol. Chem.*, **275**, 40601–40604.
22. Luo,W., Muller,J.G., Rachlin,E.M. and Burrows,C.J. (2000) Characterization of spiroiminodihydantoin as a product of one-electron oxidation of 8-oxo-7,8-dihydroguanosine. *Org. Lett.*, **2**, 613–616.
23. Luo,W., Muller,J.G., Rachlin,E.M. and Burrows,C.J. (2001) Characterization of hydantoin products from one-electron oxidation of 8-oxo-7,8-dihydroguanosine in a nucleoside model. *Chem. Res. Toxicol.*, **14**, 927–938.
24. Duarte,V., Gasparutto,D., Yamaguchi,L.F., Ravanat,J.L., Martinez,G.R., Medeiros,M.H.G., Di Mascio,P. and Cadet,J. (2000) Oxaluric acid as the major product of singlet oxygen-mediated oxidation of 8-oxo-7,8-dihydroguanine in DNA. *J. Am. Chem. Soc.*, **122**, 12622–12628.
25. Kino,K. and Saito,I. (1998) Product analysis of GG-specific photooxidation of DNA via electron transfer: 2-aminoimidazolone as a major guanine oxidation product [14]. *J. Am. Chem. Soc.*, **120**, 7373–7374.
26. Kawai,K., Osakada,Y., Fujitsuka,M. and Majima,T. (2005) Consecutive adenine sequences are potential targets in photosensitized DNA damage. *Chem. Biol.*, **12**, 1049–1054.
27. Arnold,A.R., Grodick,M.A. and Barton,J.K. (2016) DNA Charge Transport: From Chemical Principles to the Cell. *Cell Chem. Biol.*, **23**, 183–197.
28. Liu,Z., Gao,Y. and Wang,Y. (2003) Identification and characterization of a novel cross-link lesion in d(CpC) upon 365-nm irradiation in the presence of 2-methyl-1, 4-naphthoquinone. *Nucleic Acids Res.*, **31**, 5413–5424.
29. Crean,C., Uvaydov,Y., Geacintov,N.E. and Shafirovich,V. (2008) Oxidation of single-stranded oligonucleotides by carbonate radical anions: Generating intrastrand cross-links between guanine and thymine bases separated by cytosines. *Nucleic Acids Res.*, **36**, 742–755.

30. Rozelle,A.L., Cheun,Y., Vilas,C.K., Koag,M.C. and Lee,S. (2021) DNA interstrand cross-links induced by the major oxidative adenine lesion 7,8-dihydro-8-oxoadenine. *Nat. Commun.*, **12**, 1–16.
31. Bauer,N.C., Corbett,A.H. and Doetsch,P.W. (2015) The current state of eukaryotic DNA base damage and repair. *Nucleic Acids Res.*, **43**, 10083–10101.
32. Lindahl,T., Karran,P. and Wood,R.D. (1997) DNA excision repair pathways. *Curr. Opin. Genet. Dev.*, **7**, 158–169.
33. Trasviña-Arenas,C.H., Demir,M., Lin,W.J. and David,S.S. (2021) Structure, function and evolution of the Helix-hairpin-Helix DNA glycosylase superfamily: Piecing together the evolutionary puzzle of DNA base damage repair mechanisms. *DNA Repair (Amst).*, **108**.
34. Sites,A.A., Loeb,L.A. and Preston,B.D. (1986) Mutagenesis by apurinic/apyrimidinic sites. *Annu. Rev. Genet.*, **20**, 201– 230.
35. Wilson,D.M. and Barsky,D. (2001) The major human abasic endonuclease: Formation, consequences and repair of abasic lesions in DNA. *Mutat. Res. - DNA Repair*, **485**, 283–307.
36. Lindahl,T. and Nyberg,B. (1972) Rate of Depurination of Native Deoxyribonucleic Acid. *Biochemistry*, **11**, 3610–3618.
37. Guillet,M. and Boiteux,S. (2003) Origin of Endogenous DNA Abasic Sites in Saccharomyces cerevisiae . *Mol. Cell. Biol.*, **23**, 8386–8394.
38. Boiteux,S. and Guillet,M. (2004) Abasic sites in DNA: Repair and biological consequences in Saccharomyces cerevisiae. *DNA Repair (Amst).*, **3**, 1–12.
39. Dutta,S., Chowdhury,G. and Gates,K.S. (2007) Interstrand cross-links generated by abasic sites in duplex DNA. *J. Am. Chem. Soc.*, **129**, 1852–1853.
40. Johnson,K.M., Price,N.E., Wang,J., Fekry,M.I., Dutta,S., Seiner,D.R., Wang,Y. and Gates,K.S. (2013) On the formation and properties of interstrand DNA-DNA cross-links forged by reaction of an abasic site with the opposing guanine residue of 5′-CAp sequences in duplex DNA. *J. Am. Chem. Soc.*, **135**, 1015–1025.
41. Sczepanski,J.T., Wong,R.S., McKnight,J.N., Bowman,G.D. and Greenberg,M.M. (2010) Rapid DNA-protein cross-linking and strand scission by an abasic site in a nucleosome core particle. *Proc. Natl. Acad. Sci. U. S. A.*, **107**, 22475–22480.

42. Halabelian,L., Ravichandran,M., Li,Y., Zeng,H., Rao,A., Aravind,L. and Arrowsmith,C.H. (2019) Structural basis of HMCES interactions with abasic DNA and multivalent substrate recognition. *Nat. Struct. Mol. Biol.*, **26**, 607–612.

43. Wilson,D.L. and Kool,E.T. (2019) Ultrafast Oxime Formation Enables Efficient Fluorescence Light-up Measurement of DNA Base Excision. *J. Am. Chem. Soc.*, **141**, 19379–19388.

44. Jun,Y.W., Harcourt,E.M., Xiao,L., Wilson,D.L. and Kool,E.T. (2022) Efficient DNA fluorescence labeling via base excision trapping. *Nat. Commun.*, **13**.

45. Takada,T., Ido,M., Ashida,A., Nakamura,M. and Yamana,K. (2016) DNA-Templated Synthesis of Perylenediimide Stacks Utilizing Abasic Sites as Binding Pockets and Reactive Sites. *ChemBioChem*, **17**, 2230–2233.

46. Takada,T., Ishino,S., Takata,A., Nakamura,M., Fujitsuka,M., Majima,T. and Yamana,K. (2018) Rapid Electron Transfer of Stacked Heterodimers of Perylene Diimide Derivatives in a DNA Duplex. *Chem. - A Eur. J.*, **24**, 8228–8232.

47. Ichikawa,K., Kojima,N., Hirano,Y., Takebayashi,T., Kowata,K. and Komatsu,Y. (2012) Interstrand cross-link of DNA by covalently linking a pair of abasic sites. *Chem. Commun.*, **48**, 2143–2145.

48. Mie,Y., Hirano,Y., Kowata,K., Nakamura,A., Yasunaga,M., Nakajima,Y. and Komatsu,Y. (2018) Function Control of Anti-microRNA Oligonucleotides Using Interstrand Cross-Linked Duplexes. *Mol. Ther. Nucleic Acids*, **10**, 64–74.

49. Yoshimoto,K., Nishizawa,S., Minagawa,M. and Teramae,N. (2003) Use of abasic site-containing DNA strands for nucleobase recognition in water. *J. Am. Chem. Soc.*, **125**, 8982–8983.

50. Sankaran,N.B., Nishizawa,S., Seino,T., Yoshimoto,K. and Teramae,N. (2006) Abasic-site-containing oligodeoxynucleotides as aptamers for riboflavin. *Angew. Chemie - Int. Ed.*, **45**, 1563–1568.

51. Sato,N., Tsuji,G., Sasaki,Y., Usami,A., Moki,T., Onizuka,K., Yamada,K. and Nagatsugi,F. (2015) A new strategy for site-specific alkylation of DNA using oligonucleotides containing an abasic site and alkylating probes. *Chem. Commun.*, **51**, 14885–14888.

52. Liu,Z.J., Martínez Cuesta,S., van Delft,P. and Balasubramanian,S. (2019) Sequencing abasic sites in DNA at single-nucleotide resolution. *Nat. Chem.*, **11**, 629–637.

53. Yamano,Y., Onizuka,K., Sasaki,M., Sato,S. and Nagatsugi,F. (2022) Photochemical Labeling of Nucleic Acid by Photocatalyst Tethered DNA Probe. *Chem. Lett.*, **51**, 1121–1124.

54. R Wing, H Drew, T Takano, C Broka, S Tanaka, K Itakura,R.E.D. (1980) Crystal structure analysis of a complete turn of B-DNA. *Nature*, **287**, 755–758.

55. Ye,Y., Muller,J.G., Luo,W., Mayne,C.L., Shallop,A.J., Jones,R.A. and Burrows,C.J. (2003) Formation of 13C-, 15N-, and 18O-Labeled Guanidinohydantoin from Guanosine Oxidation with Singlet Oxygen. Implications for Structure and Mechanism. *J. Am. Chem. Soc.*, **125**, 13926–13927.

56. Robson,C.N. and Hickson,I.D. (1991) Isolation of cDNA clones encoding a human apurini/apyrimidinic endonuclease that corects DNA repair and mutagenisis defects in E.coli xth (exonuclease III) mutants. *Nucleic Acids Res.*, **19**, 5519–5523.

57. Fleming,A.M., Alshykhly,O., Zhu,J., Muller,J.G. and Burrows,C.J. (2015) Rates of Chemical Cleavage of DNA and RNA Oligomers Containing Guanine Oxidation Products. *Chem. Res. Toxicol.*, **28**, 1292–1300.

58. Harbour,J.R. and Issler,S.L. (1982) Involvement of the azide radical in the quenching of singlet oxygen by azide anion in water. *J. Am. Chem. Soc*, **104**, 903–905.

59. Costa,L., Faustino,M.A.F., Tomé,J.P.C., Neves,M.G.P.M.S., Tomé,A.C., Cavaleiro,J.A.S., Cunha,Â. and Almeida,A. (2013) Involvement of type i and type II mechanisms on the photoinactivation of non-enveloped DNA and RNA bacteriophages. *J. Photochem. Photobiol. B Biol.*, **120**, 10–16.

60. Kanamori,T., Kaneko,S., Hamamoto,K. and Yuasa,H. (2023) Mapping the diffusion pattern of 1O2 along DNA duplex by guanine photooxidation with an appended biphenyl photosensitizer. *Sci. Rep.*, **13**, 1–10.

61. Schweitzer,C. and Schmidt,R. (2003) Physical mechanisms of generation and deactivation of singlet oxygen. *Chem. Rev.*, **103**, 1685–1757.

62. Park,J.H., Troxel,A.B., Harvey,R.G. and Penning,T.M. (2006) Polycyclic aromatic hydrocarbon (PAH) o-quinones produced by the Aldo-Keto-Reductases (AKRs) generate abasic sites, oxidized pyrimidines, and 8-Oxo-dGuo via reactive oxygen species. *Chem. Res. Toxicol.*, **19**, 719–728.

63. Ouchi,A., Aizawa,K., Iwasaki,Y., Inakuma,T., Terao,J., Nagaoka,S.I. and Mukai,K. (2010) Kinetic study of the quenching reaction of singlet oxygen by carotenoids and food extracts in solution. development of a singlet oxygen absorption capacity (SOAC) assay method. *J. Agric. Food Chem.*, **58**, 9967–9978.

64. Ashwood,B., Jones,M.S., Lee,Y., Sachleben,J.R., Ferguson,A.L. and Tokmakoff,A. (2024) Molecular insight into how the position of an abasic site modifies DNA duplex stability and dynamics. *Biophys. J.*, **123**, 118–133.

65. McCallum,J.E.B., Kuniyoshi,C.Y. and Foote,C.S. (2004) Characterization of 5-hydroxy-8-oxo-7,8-dihydroguanosine in the photosensitized oxidation of 8-oxo-7,8-dihydroguanosine and its rearrangement to spiroiminodihydantoin. *J. Am. Chem. Soc.*, **126**, 16777–16782.

66. Raoul,S. and Cadet,J. (1996) Photosensitized reaction of 8-oxo-7,8-dihydro-2′-deoxyguanosine: Identification of 1-(2-deoxy-β-D-erythro-pentofuranosyl)cyanuric acid as the major singlet oxygen oxidation product. *J. Am. Chem. Soc.*, **118**, 1892–1898.

67. Stathis,D., Lischke,U., Koch,S.C., Deiml,C.A. and Carell,T. (2012) Discovery and mutagenicity of a guanidinoformimine lesion as a new intermediate of the oxidative deoxyguanosine degradation pathway. *J. Am. Chem. Soc.*, **134**, 4925–4930.

68. Sodum,R.S., Nie,G. and Fiala,E.S. (1993) 18-Aminoguanine: A Base Modification Produced in Rat Liver Nucleic Acids by the Hepatocarcinogen 2-Nitropropane. *Chem. Res. Toxicol.*, **6**, 269–276.

69. Xu,X., Muller,J.G., Ye,Y. and Burrows,C.J. (2008) DNA-protein cross-links between guanine and lysine depend on the mechanism of oxidation for formation of C5 vs C8 guanosine adducts. *J. Am. Chem. Soc.*, **130**, 703–709.

70. Rozelle,A.L. and Lee,S. (2021) Genotoxic C8-Arylamino-2′-deoxyadenosines Act as Latent Alkylating Agents to Induce DNA Interstrand Cross-Links. *J. Am. Chem. Soc.*, **143**, 18960–18976.

71. Shibutani,S., Gentles,R.G., Iden,C.R. and Johnson,F. (1990) Facile aerial oxidation of the DNA-base adduct N-(2′-deoxyguanosin-8-yl)-2-aminofluorene [dG(C8)AF]. *J. Am. Chem. Soc.*, **112**, 5667–5668.

72. Garrett,E.R., Seydel,J.K. and Sharpen,A.J. (1966) The Acid-Catalyzed Solvolysis of Pyrimidine Nucleosides1. *J. Org. Chem.*, **31**, 2219–2227.

73. Liu,Y., Rodriguez,Y., Ross,R.L., Zhao,R., Watts,J.A., Grunseich,C., Bruzel,A., Li,D., Burdick,J.T., Prasad,R., *et al.* (2020) RNA abasic sites in yeast and human cells. *Proc. Natl. Acad. Sci. U. S. A.*, **117**, 20689–20695.